

Non-Abelian Braiding of Chiral Majorana Fermions by Quantum Dots

Yan-Feng Zhou^{1,2}, Zhe Hou^{1,2}, and Qing-Feng Sun^{1,2,3*}

¹*International Center for Quantum Materials, School of Physics, Peking University, Beijing 100871, China*

²*Collaborative Innovation Center of Quantum Matter, Beijing 100871, China and*

³*CAS Center for Excellence in Topological Quantum Computation, University of Chinese Academy of Sciences, Beijing 100190, China*

(Dated: November 9, 2018)

The non-Abelian braiding of Majorana fermions is one of the most promising operations providing a key building block for the realization of topological quantum computation. Recently, the chiral Majorana fermions were observed in a hybrid junction between a quantum anomalous Hall insulator and an s-wave superconductor. Here we show that if a quantum dot or Majorana zero mode couples to the chiral Majorana fermions, the resulting resonant exchange of chiral Majorana fermions can lead to the non-Abelian braiding. Remarkably, any operation in the braid group can be achieved by this scheme. We further propose electrical transport experiments to observe the braiding of four chiral Majorana fermions and demonstrate the non-Abelian braiding statistics in four-terminal devices of the hybrid junctions. Both a conductance peak due to the braiding and the braiding-order dependent conductance are predicted. These findings pave a way to perform any braiding operation of chiral Majorana fermions by electrically controllable quantum dots.

Majorana fermion with antiparticle being itself, is originally introduced as a putative elementary particle by Ettore Majorana, and has been now pursued as quasiparticle excitation in condensed-matter systems [1–3]. Quantum information can be stored nonlocally in the degenerate ground state space generated by the zero-energy Majorana excitations. Because of the non-Abelian braiding statistics [4, 5], that information can be manipulated through the exchange of the Majorana excitations which leads to a noncommutative transformation between different ground states. The final state is determined by the topology of the braiding and is robust against local perturbation, with possible applications in topological quantum computation [6–10].

For the zero-dimensional case, Majorana zero modes (MZMs) are predicted as midgap states bound to charge- $e/4$ quasiparticles of $\nu = 5/2$ fractional quantum Hall effect [4, 11–13] and Abrikosov vortices in topological superconductors (TSCs) [5, 14–16]. Moreover, alternative proposals suggest that a semiconducting nanowire coupled with a superconductor can also support MZMs localized at the wire ends [17–19] and mounting experimental progress in pursuing MZMs in these systems has been achieved by measuring the zero-bias peak of tunneling spectroscopy [20–23]. Despite the architectures proposed for performing the braiding operations of MZMs [10, 24–26], the experimental realization remains an on-going challenge.

As one-dimensional analogue of MZMs, chiral Majorana fermions emerge as unidirectionally propagating edge modes surrounding the edge of $p + ip$ TSC [15, 27–31]. The TSC has a full pairing gap classified by topological Chern number \mathcal{N} which also determines the number of chiral Majorana edge modes. Theoretical proposals show that such an exotic superconductivity could arise by bringing certain topological matters in proximity to an s-wave superconductor [15, 28]. By coupling

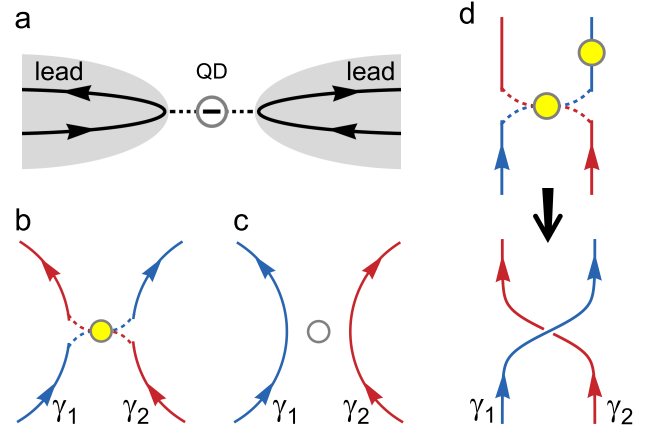


Fig. 1. Braiding of chiral Majorana fermions coupled to MZMs. With inspiration of the resonant tunneling in the lead/QD/lead model depicted in **a**, a system consisting of two chiral Majorana fermions coupled to MZMs (yellow solid circle) is proposed to braid chiral Majorana fermions as shown in **b** and **d**. When the MZM is absent or disabled as indicated by a hollow circle in **c**, the chiral Majorana fermions γ_1 (blue arrow) and γ_2 (red arrow) propagate independently. With the presence of a MZM, a resonant exchange sends $\gamma_1 \rightarrow -\gamma_2$ and $\gamma_2 \rightarrow -\gamma_1$ as shown in **b**. Moreover, a single chiral Majorana fermions coupled to a MZM will acquire a negative sign. The braiding according to $\gamma_1 \rightarrow \gamma_2$ and $\gamma_2 \rightarrow -\gamma_1$ can be realized if one couples two MZMs to $\gamma_{1,2}$ as shown in **d**.

Nb superconductor to a quantum anomalous Hall insulator (QAHI) realized in magnetic topological insulator thin films [32, 33], a half-integer conductance plateau resulting from the chiral Majorana fermion was experimentally observed [34], serving as a hopeful signature of TSC with $\mathcal{N} = 1$. Recently, one group [35] recognized that the propagation of chiral Majorana fermions can lead to braiding for performing topological quantum computations similar to the braiding of MZMs. In

contrast to bounded MZM, the chiral Majorana fermion is extended providing a promising platform for scalable quantum computations.

Motivated by the resonant tunneling of an electron through a quantum dot (QD) in the lead/QD/lead system [36] as shown in Fig.1a, we first show that if two chiral Majorana fermions $\gamma_{1,2}$ are coupled to a MZM, the resonant tunneling of Majorana fermions occurs and leads to that a resonant exchange sends $\gamma_1 \rightarrow -\gamma_2$ and $\gamma_2 \rightarrow -\gamma_1$ (see Fig.1b). On the other hand, a single chiral Majorana fermion coupled with a MZM acquires a negative sign. Our key idea is that by combining these two effects due to the coupling with MZMs (see Fig.1d), γ_1 and γ_2 are transformed according to $\gamma_1 \rightarrow \gamma_2$ and $\gamma_2 \rightarrow -\gamma_1$, reminiscent of the braiding of MZMs. Then we demonstrate that such braiding of chiral Majorana fermions could be completely reproduced by replacing MZMs with QDs, which are well constructed and can be controlled by gate voltage in experiments[37–39]. We further propose a four-terminal setup of the hybrid TSC/QAHI junction to observe the braiding of four chiral Majorana fermions indicated by a resonant conductance peak. Remarkably, our proposed system can be extended to carry out any braiding operation in the braid group. For sequential exchanging process, the resonant conductance peak has a value of $\frac{e^2}{2h}$ or $\frac{e^2}{h}$ depending on the exchanging order which means the non-Abelian braiding statistics.

We begin by investigating the MZM coupling case in which a MZM is coupled to a pair of chiral Majorana fermions as shown in Fig.1b. The low energy Hamiltonian of two decoupled chiral Majorana fermions is

$$H_0 = i\nu \sum_{\alpha=1,2} \int_{-\infty}^{+\infty} \gamma_{\alpha}(x) \partial_x \gamma_{\alpha}(x) dx, \quad (1)$$

where $\gamma_{\alpha}(x)$ is the field operators of chiral Majorana fermions with $\gamma_{\alpha}^{\dagger}(x) = \gamma_{\alpha}(x)$ satisfying $\{\gamma_{\alpha}(x), \gamma_{\beta}(x')\} = \delta_{\alpha\beta} \delta_{xx'}$, and ν denotes the Fermi velocity. Let H_M describe the coupling term between the MZM γ_0 ($\gamma_0^{\dagger} = \gamma_0$ and $\{\gamma_0, \gamma_0\} = 1$) and $\gamma_{\alpha}(x)$ at $x = 0$ with a strength t_{α} . Then the total Hamiltonian is

$$H_1 = H_0 + H_M, \quad (2)$$

where $H_M = \sum_{\alpha=1,2} i t_{\alpha} \gamma_{\alpha}(0) \gamma_0$.

When MZM γ_0 is absent as denoted by a hollow circle in Fig.1c, γ_1 and γ_2 propagate independently determined by H_0 . If we switch on γ_0 as indicated by a yellow solid circle in Fig.1b, the scattering between γ_1 and γ_2 occurs at $x = 0$ due to the coupling with a MZM. In order to study the transport process, we first calculate the scattering matrix of the chiral Majorana fermions described by H_1 in Eq.(2). Denoting the incoming and outgoing scattering states of the chiral Majorana fermions by $\gamma_{1/2}(0^-)$ and $\gamma_{1/2}(0^+)$, respectively, the scattering matrix can be

written as [40]

$$\begin{pmatrix} \gamma_1(0^+) \\ \gamma_2(0^+) \end{pmatrix} = S_M \begin{pmatrix} \gamma_1(0^-) \\ \gamma_2(0^-) \end{pmatrix}, \quad (3)$$

where

$$S_M = \frac{1}{A} \begin{pmatrix} 4i\varepsilon\nu + t_1^2 - t_2^2 & -2t_1 t_2 \\ -2t_1 t_2 & 4i\varepsilon\nu + t_1^2 - t_2^2 \end{pmatrix}, \quad (4)$$

in which $A = 4i\varepsilon\nu + t_1^2 + t_2^2$ and ε is the incident energy. The off-diagonal elements of S_M matrix correspond to the amplitude for transmission between γ_1 and γ_2 . The resulting transmission coefficient is $T(\varepsilon) = |S_{M,12}|^2 = \frac{4\Gamma_1\Gamma_2}{4\varepsilon^2 + (\Gamma_1 + \Gamma_2)^2}$ with $\Gamma_{\alpha} \equiv t_{\alpha}^2/(2\nu)$ which is same with the Breit-Wigner formula describing the resonant scattering of the lead/QD/lead system.

Similar to the resonant tunneling process in the lead/QD/lead system [36] (see Fig.1a), if the value of ε largely deviates from zero, the energy mismatch disables MZM γ_0 and no transmission happens with $T = 0$ as illustrated in Fig.1c. However, it is obvious from Eq.(11) that when $\varepsilon = 0$ and $t_1 = t_2 = t$, the scattering matrix becomes $S_M = \begin{pmatrix} 0 & -1 \\ -1 & 0 \end{pmatrix}$. In other words, when the energy of the incoming chiral Majorana fermions matches the energy of the MZM, there occurs a resonant exchange according to $\gamma_1 \rightarrow -\gamma_2$ and $\gamma_2 \rightarrow -\gamma_1$ as depicted in Fig.1b. Moreover, we consider the case that γ_0 is only coupled with γ_1 by setting $t_2 = 0$ and $t_1 = t$. Here, for $\varepsilon = 0$, the scattering matrix becomes $S_M = \begin{pmatrix} -1 & 0 \\ 0 & 1 \end{pmatrix}$. This means that the phase of chiral Majorana fermion can be changed by a value of π as $\gamma_1 \rightarrow -\gamma_1$, which can be also realized by the coupling with a metallic island [31]. More interestingly, it can be shown that two successive manipulations in which one MZM is first coupled simultaneously to γ_1 and γ_2 , and then an additional one is coupled solely to γ_1 (see Fig.1d), can recover the braiding of chiral Majorana fermions, $\gamma_1 \rightarrow \gamma_2$ and $\gamma_2 \rightarrow -\gamma_1$, as that in the braiding of MZMs. At this point, it suggests that our method makes the braiding of chiral Majorana fermions possible with the coupling of MZMs.

Considering that a zero-energy charged fermion bound state is topologically equivalent to a pair of MZMs [1], whether a QD with a single energy level can provide an alternative approach to braid the chiral Majorana fermions as well as MZM. Next, we consider that two chiral Majorana fermions are coupled to a QD as shown in Fig.2a. The total Hamiltonian now becomes

$$H_2 = H_0 + H_{QD} + H_C, \quad (5)$$

where $H_{QD} = \varepsilon_d d^{\dagger} d$ and $H_C = \sum_{\alpha=1,2} i(\tilde{t}_{\alpha}/\sqrt{2}) \gamma_{\alpha}(0)(d + d^{\dagger})$ [41]. The second term H_{QD} is the Hamiltonian of the QD with a single energy level ε_d and d^{\dagger} (d) are the creation (annihilation) operators of the fermion state in the QD. The third term H_C describes the coupling between γ_{α} and the QD with a coupling strength \tilde{t}_{α} .

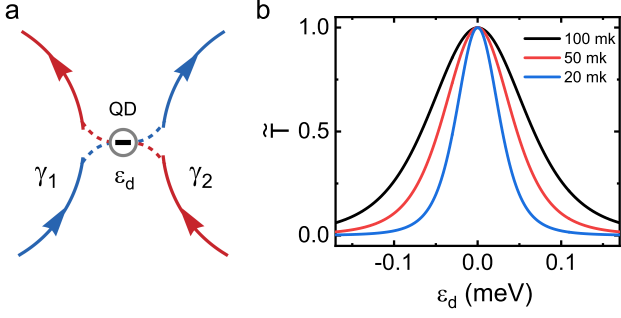


Fig. 2. Electrical control of the braiding of chiral Majorana fermions coupled to a QD. Considering that a zero-energy charged fermion is topologically equivalent to a pair of MZMs, a system consisting of two chiral Majorana fermions coupled to a QD with a single energy level ε_d in **a** is demonstrated to be able to braid chiral Majorana fermions as well as in Fig.1c. **b**, The transmission \tilde{T} describing the scattering between γ_1 and γ_2 due to the QD coupling as a function of ε_d at different temperatures. In real experiments, ε_d inside the QD can be tuned by gate voltages. For $\varepsilon_d = 0$, the resonant exchange of γ_1 and γ_2 occurs ($\tilde{T} = 1$).

In this case, the scattering matrix denoted by S_Q becomes [40]

$$S_Q = \frac{1}{\tilde{A}} \begin{pmatrix} \tilde{B} + \tilde{t}_2^2 - \tilde{t}_1^2 & -2\tilde{t}_1\tilde{t}_2 \\ -2\tilde{t}_1\tilde{t}_2 & \tilde{B} + \tilde{t}_1^2 - \tilde{t}_2^2 \end{pmatrix}, \quad (6)$$

where $\tilde{B} = 4i\nu(\varepsilon^2 - \varepsilon_d^2)/\varepsilon$ and $\tilde{A} = \tilde{B} + \tilde{t}_1^2 + \tilde{t}_2^2$. For comparison with the MZM setting $\varepsilon_d = 0$, it can be found that the scattering matrix S_Q is the same as S_M in Eq.(11). Therefore, the QD should be able to accomplish the braiding of chiral Majorana fermions as the MZM. On the other hand, in real experiments the energy level ε_d inside the QD can be tuned easily by gate voltages [37–39]. For finite ε_d , the transmission coefficient now becomes $\tilde{T}(\varepsilon) = |S_{Q,12}|^2 = \frac{4\tilde{\Gamma}_1\tilde{\Gamma}_2}{4(\varepsilon^2 - \varepsilon_d^2)^2 + (\tilde{\Gamma}_1 + \tilde{\Gamma}_2)^2}$ with $\tilde{\Gamma}_\alpha \equiv \tilde{t}_\alpha^2/(2\nu)$. Considering the non-zero temperature \mathcal{T} , the effective transmission coefficient is $\tilde{T} = \int_{-\infty}^{+\infty} \tilde{T}(\varepsilon) f(\varepsilon) d\varepsilon$, in which $f(\varepsilon) = [\exp(\varepsilon/k_B\mathcal{T}) + 1]^{-1}$ is the Fermi distribution function. Fig.2b shows \tilde{T} as functions of ε_d with $\tilde{\Gamma}_1 = \tilde{\Gamma}_2 \equiv \Gamma = 1$ meV at different temperatures. It can be seen that the transmission curves \tilde{T} show obviously resonant behaviors with a peak at $\varepsilon_d = 0$ where the resonant exchange of chiral Majorana fermions occurs. If the value of ε_d deviates from zero, \tilde{T} decreases with a full-width at half-maximum estimated to be $\sqrt{\Gamma k_B\mathcal{T}}$. When ε_d is far from zero, \tilde{T} tends to zero and the chiral Majorana fermions propagate independently without exchange as shown in Fig.1c. This result implies an electrical method to control the braiding. In contrast to MZMs, the QDs are well constructed experimentally [39] and thus the QDs are considered in the following discussion.

To observe the braiding of chiral Majorana fermions experimentally, we propose the electrical transport in a four-terminal device where two ribbons of hybrid TSC/QAHI junctions with opposite out-plane magnetization are coupled by a QD as depicted in Fig.3a. The QAHI was realized in magnetically doped topological insulators with Chern number $\mathcal{C} = 1$ and has one chiral Dirac edge mode around its boundary [32, 33]. As discussed in the introduction, the recently observed TSC has a Chern number $\mathcal{N} = 1$ which corresponds to one chiral Majorana edge mode [34]. In view of the fact that a chiral QAHI edge mode is equivalent to two chiral Majorana edge modes [28], the transport process in the device occurs via four chiral Majorana edge states γ_i ($i = 1, 2, 3, 4$) as denoted by red and blue arrows in Fig.3a. The QD between the TSC regions behaves as a switch for controlling the braiding of γ_2 and γ_3 and determines the terminal conductance.

The measured current in lead n can be calculated using the multiprobe Landauer-Büttiker formula [42–44]

$$I_n = \frac{e^2}{h} \sum_m T_{nm}(V_n - V_m) + T_{nm}^A(V_n + V_m), \quad (7)$$

where T_{nm} (T_{nm}^A) is the normal tunneling (Andreev reflection) coefficient from lead m to lead n and V_n is the voltage of terminal n . The voltage of lead 1 is fixed to V and the voltages of lead 2,3,4 have the same value (see Fig.3a). These transport coefficients can be calculated from the scattering matrix S_Q in Eq.(16) (refer to Supplementary Information [40] for a detailed derivation of these quantities). The conductance of lead n is defined as $G_n = \frac{-I_n}{V_1 - V_n}$. Fig.3b and 3c display the transport coefficients and terminal conductance as functions of ε_d , respectively. If ε_d is tuned away from zero, the electrical transports in two ribbons are independent despite the QD ($T_{41} = T_{41}^A = 0$) and the normal tunneling process dominates with $T_{31} = 1$, leading to $G_3 = e^2/h$ and $G_4 = 0$. As ε_d approaches to zero, the transmission between γ_2 and γ_3 takes place with a resonant exchange $\gamma_2 \rightarrow -\gamma_3$ and $\gamma_3 \rightarrow -\gamma_2$. In this situation, originating from lead 1, γ_1 enters into lead 3 normally and γ_2 tunnels into lead 4 due to the resonant exchange. As a result, the normal tunneling coefficient and Andreev reflection coefficient from lead 1 to both lead 3 and 4 are equal, i.e., $T_{31} = T_{31}^A = T_{41} = T_{41}^A = 1/4$ as shown in Fig.3b. Moreover, it can be seen from Fig.3c that the conductance G_4 shows a peak of $\frac{e^2}{2h}$ while G_3 has a valley of $\frac{e^2}{2h}$ with $G_2 + G_3 + G_4 = \frac{e^2}{h}$ and $G_2 = 0$.

In principle, there are infinite braiding operations on four chiral Majorana fermions forming a braid group. Any braiding operation in the group can be represented algebraically in terms of generators σ_i with $i = 1, 2, 3$ [9]. The braiding of γ_α at the i th position and γ_β at $(i+1)$ th position is a non-Abelian unitary transformation with the form $\sigma_i = \exp(\pi\gamma_\beta\gamma_\alpha/2)$. Now, we take the device

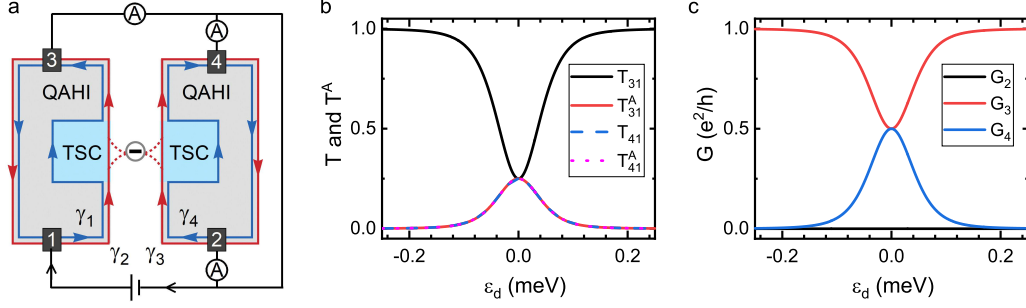


Fig. 3. Experimental device that allows the observation of the braiding based on TSC/QAHI junctions. **a**, Transport process via four chiral Majorana fermions γ_i ($i = 1, 2, 3, 4$). The chirality of γ_i in left part is different with the one in right part resulting from the opposite magnetization in two regions. The QD coupled to the TSC/QAHI junctions can trigger the exchange of γ_2 and γ_3 . **b** and **c**, Transport coefficients for the transmission process for lead 1 to lead 3 and 4, and terminal conductance as functions of ε_d . For $\varepsilon_d = 0$, the resonant exchange of γ_2 and γ_3 occurs with $T_{31} = T_{31}^A = T_{41} = T_{41}^A = 1/4$, and G_4 (G_3) shows a peak (valley).

with two ribbons of TSC/QAHI junctions in Fig.4a as an example to show our strategy to execute all the three generators. There are four chiral Majorana edge modes denoted by arrowed lines starting from leads 1 and 2. Similar to the discussion in Fig.1d, with the coupling of two successive QDs, the consequent operation completes σ_2 which braids the chiral Majorana fermions propagating along the central two red lines. Moreover, gate voltage V_G of the left ribbon in Fig.4a can induce an additional phase for the chiral QAHI edge state leading to a transformation between the chiral Majorana fermions on the first and second lines sorted from left to right, which is equivalent to the braiding operator σ_1 [35]. Similarly, generator σ_3 can be carried out by placing a gate voltage on the QAHI edge of the right ribbon. Accordingly, in view of the scalability of chiral Majorana edge modes, the proposed device provides a scalable platform to perform any braiding operation by an arbitrary combination of the three generators. Moreover, all the braiding operations can be well controlled and tuned by the electrical method [40].

With this exciting possibility to carry out any braiding operation, we next propose the electrical transport experiments in the devices as shown in Fig.4 to observe the non-Abelian braiding statistics where the sequential exchanges are executed in different orders. Here, we set $\varepsilon_d = 0$ for all the QDs. Let us define the occupation number 0 or 1 of the QAHI edge states in the left and right ribbons as two qubits L and R with bases $|0_x\rangle$ and $|1_x\rangle$ ($x = L, R$) [35]. The degenerate ground-state space of the two qubits is expanded by four states, $|0_L0_R\rangle$, $|1_L0_R\rangle$, $|0_L1_R\rangle$, and $|1_L1_R\rangle$. First, we consider two joint operators $\sigma_2\sigma_1$ and $\sigma_1\sigma_2$. After the braiding operations, the chiral Majorana fermions $(\gamma_1, \gamma_2, \gamma_3, \gamma_4)$ are transformed to $(-\gamma_2, -\gamma_3, \gamma_1, \gamma_4)$ by $\sigma_2\sigma_1$ and to $(\gamma_3, \gamma_1, \gamma_2, \gamma_4)$ by $\sigma_1\sigma_2$, respectively. If we prepare the system into an initial state $|\psi_i\rangle = |1_L0_R\rangle$ by injecting the electrons into the

qubit L one by one from lead 1 with weak current, it can be found that $\sigma_2\sigma_1$ turns the system into a final state $|\psi_{f1}\rangle = (|1_L0_R\rangle - i|0_L1_R\rangle)/\sqrt{2}$ and $\sigma_1\sigma_2$ turns it into another different state $|\psi_{f2}\rangle = (|1_L0_R\rangle - |0_L1_R\rangle)/\sqrt{2}$, correspondingly [5]. Unfortunately, the two different final states cannot be distinguished by the proposed four-terminal device in which we find $G_3 = G_4 = \frac{e^2}{2h}$ for both cases [40]. Although the two joint operators are carried out in different order, they both transport γ_1 and γ_2 coming from lead 1 to different leads (lead 3 and lead 4), respectively, and this leads to the same result of conductance measurements.

However, the operators constituted by three sequential exchanges $\sigma_2\sigma_1\sigma_2$ and $\sigma_2\sigma_2\sigma_1$ in Fig.4 yields very different results, indicating the non-Abelian braiding statistics. In this situation, $(\gamma_1, \gamma_2, \gamma_3, \gamma_4)$ are transformed to $(\gamma_3, -\gamma_2, \gamma_1, \gamma_4)$ by $\sigma_2\sigma_1\sigma_2$ and to $(-\gamma_2, -\gamma_1, -\gamma_3, \gamma_4)$ by $\sigma_2\sigma_2\sigma_1$ as shown in the middle part of Fig.4. From the initial state $|\psi_i\rangle = |1_L0_R\rangle$, the device in Fig.4a arrives at the final state $|\psi_{f2}\rangle = (|1_L0_R\rangle - |0_L1_R\rangle)/\sqrt{2}$ transformed by $\sigma_2\sigma_1\sigma_2$ while the joint operator $\sigma_2\sigma_2\sigma_1$ drives the device in Fig.4b into a final state $|\psi_{f3}\rangle = |0_L1_R\rangle$ [5]. As a result, the conductances observed in Fig.4a are $G_3 = G_4 = \frac{e^2}{2h}$, but the ones in Fig.4b are $G_4 = \frac{e^2}{h}$ and $G_3 = 0$ [40]. In the case of $\sigma_2\sigma_2\sigma_1$, γ_1 and γ_2 enter into lead 3 together, and recombine as a hole providing a different conductance measurement. These results provide a signature supporting the non-Abelian braiding statistics of chiral Majorana fermions.

To conclude, we proposed a new method to perform any braiding operation of chiral Majorana fermions coupled with QDs or MZMs and proposed electrical transport experiments to observe both the braiding and its non-Abelian statistics. Considering that the pursuit of topological states which support quasiparticle excitations obeying non-Abelian statistics is one of the most important issues in topological quantum computation, the abil-

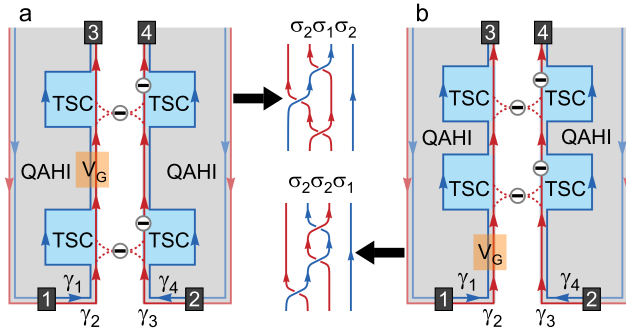


Fig. 4. Experimental devices providing a demonstration for the non-Abelian braiding statistics. To observe the non-Abelian statistics of the braiding in the electrical transport, one has to perform sequential exchanges and demonstrate that the measurement results of the device are dependent on the braiding order. The gate voltage V_G performs the operator σ_1 and the operator σ_2 is carried out by two successive QDs as discussed in Fig.1d. Two joint operations constituted by three sequential exchanges, $\sigma_2\sigma_1\sigma_2$ as realized in **a** and $\sigma_2\sigma_2\sigma_1$ as realized in **b**, turn the systems into completely different final states and yield different measurement results of the terminal conductances. The middle part shows the corresponding braiding of γ_i ($i = 1, 2, 3, 4$) in the two devices.

ity to realize the non-Abelian braiding of chiral Majorana fermions in our proposed devices is remarkable. Moreover, for any required unitary transformations, the braiding operations can be carried out by directly extending the hybrid TSC/QAHI devices and can well be controlled and tuned by the electrical method. This braiding scheme provide a convincing signature of chiral Majorana fermions and pave a feasible way towards the topological quantum computation.

* sunqf@pku.edu.cn

- [1] Alicea J. New directions in the pursuit of Majorana fermions in solid state systems. *Rep. Prog. Phys.* **75**, 076501 (2012).
- [2] Beenakker C.W.J. Search for Majorana fermions in superconductors. *Annu. Rev. Condens. Matter Phys.* **4**, 113 (2013).
- [3] Das Sarma, S., Freedman, M. & Nayak, C. Majorana zero modes and topological quantum computation. *npj Quantum Information* **1**, 15001 (2015).
- [4] Read, N. & Green, D. Paired states of fermions in two dimensions with breaking of parity and time-reversal symmetries and the fractional quantum Hall effect. *Phys. Rev. B* **61**, 10267 (2000).
- [5] Ivanov, D. A. Non-Abelian statistics of half-quantum vortices in p-wave superconductors. *Phys. Rev. Lett.* **86**, 268 (2001).
- [6] Kitaev, A. Fault-tolerant quantum computation by anyons. *Ann. Phys.* **303**, 230 (2003).
- [7] Freedman, M.H., Larsen, M. & Wang, Z. A modular func-

tor which is universal for quantum computation. *Commun. Math. Phys.* **227**, 605 (2002).

- [8] Das Sarma, S., Freedman, M. & Nayak, C. Topologically protected qubits from a possible non-Abelian fractional quantum Hall state. *Phys. Rev. Lett.* **94**, 166802 (2005).
- [9] Nayak, C., Simon, S. H., Stern, A., Freedman, M. & Das Sarma, S. Non-Abelian anyons and topological quantum computation. *Rev. Mod. Phys.* **80**, 10831159 (2008).
- [10] Alicea J., Oreg Y., Refael G., von Oppen F. & Fisher M.P.A., Non-Abelian statistics and topological quantum information processing in 1D wire networks *Nat. Phys.* **7**, 412-417 (2011).
- [11] Moore, G. & Read, N. Nonabelions in the fractional quantum Hall effect. *Nucl. Phys. B* **360**, 362396 (1991).
- [12] Radu, I.P., Miller, J.B., Marcus, C.M., Kastner, M.A., Pfeiffer, L.N. & West, K.W. Quasi-particle properties from tunneling in the $\nu = 5/2$ fractional quantum Hall state. *Science* **320**, 899-902 (2008).
- [13] Dolev, M., Heiblum, M., Umansky, V., Stern, A. & Mahalu, D. Observation of a quarter of an electron charge at the $\nu = 5/2$ quantum Hall state. *Nature* **452**, 829-834 (2008).
- [14] Volovik G.E. Fermion zero modes on vortices in chiral superconductors. *Soviet J. Exp. Theor. Phys. Letters* **70**, 609-614 (1999).
- [15] Fu, L. & Kane, C.L. Superconducting proximity effect and Majorana fermions at the surface of a topological insulator. *Phys. Rev. Lett.* **100**, 096407 (2008).
- [16] Sun, H.-H. *et al.* Majorana zero mode detected with spin selective Andreev reflection in the vortex of a topological superconductor. *Phys. Rev. Lett.* **116**, 257003 (2016).
- [17] Kitaev, A. Y. Unpaired Majorana fermions in quantum wires. *Phys.-Usp.* **44**, 131136 (2001).
- [18] Lutchyn, R. M., Sau, J. D. & Das Sarma, S. Majorana fermions and a topological phase transition in semiconductor-superconductor heterostructures. *Phys. Rev. Lett.* **105**, 077001 (2010).
- [19] Oreg, Y., Refael, G. & von Oppen, F. Helical liquids and Majorana bound states in quantum wires. *Phys. Rev. Lett.* **105**, 177002 (2010).
- [20] Mourik, V. *et al.* Signatures of Majorana fermions in hybrid superconductor-semiconductor nanowire devices. *Science* **336**, 1003-1007 (2012).
- [21] Das, A. Zero-bias peaks and splitting in an Al-InAs nanowire topological superconductor as a signature of Majorana fermions. *Nat. Phys.* **8**, 887-895 (2012).
- [22] Deng, M. T. *et al.* Majorana bound state in a coupled quantum-dot hybrid nanowire system. *Science* **354**, 1557-1562 (2016).
- [23] Zhang, H. *et al.* Quantized Majorana conductance. *Nature* **556**, 74-79 (2018).
- [24] Hyart, T. *et al.* Flux-controlled quantum computation with Majorana fermions. *Phys. Rev. B* **88**, 035121 (2013).
- [25] Plugge, S., Rasmussen, A., Egger, R. & Flensberg, K. Majorana box qubits. *New J. Phys.* **19**, 012001 (2016).
- [26] Karzig, T. Scalable designs for quasiparticle-poisoning-protected topological quantum computation with Majorana zero modes. *Phys. Rev. B* **95**, 235305 (2017).
- [27] Mackenzie, A.P. & Maeno, Y. The superconductivity of Sr_2RuO_4 and the physics of spin-triplet pairing. *Rev. Mod. Phys.* **75**, 657-712 (2003).
- [28] Qi, X.-L., Hughes, T. L. & Zhang, S.-C. Chiral topological superconductor from the quantum Hall state. *Phys. Rev.*

- B* **82**, 184516 (2010).
- [29] Sau, J. D., Lutchyn, R. M., Tewari, S. & Das Sarma, S. Generic new platform for topological quantum computation using semiconductor heterostructures. *Phys. Rev. Lett.* **104**, 040502 (2010).
 - [30] Wang, J., Zhou, Q., Lian, B. & Zhang, S.-C. Chiral topological superconductor and half-integer conductance plateau from quantum anomalous Hall plateau transition. *Phys. Rev. B* **92**, 064520 (2015).
 - [31] Zhou, Y.-F., Hou, Z., Zhang, Y.-T. & Sun, Q.-F. Chiral Majorana fermion modes regulated by a scanning tunneling microscope tip. *Phys. Rev. B* **97**, 115452 (2018).
 - [32] Chang, C.-Z. *et al.* Experimental observation of the quantum anomalous Hall effect in a magnetic topological insulator. *Science* **340**, 167-170 (2013).
 - [33] Kandala, A., Richardella, A., Kempinger, S., Liu, C.-X. & Samarth, N. Giant anisotropic magnetoresistance in a quantum anomalous Hall insulator. *Nat. Commun.* **6**, 7434 (2015).
 - [34] He, Q.L. *et al.* Chiral Majorana fermion modes in a quantum anomalous Hall insulator/superconductor structure. *Science* **357**, 294-299 (2017).
 - [35] Lian, B., Sun, X.-Q., Vaezi, A., Qi, X.-L. & Zhang, S.-C. Topological quantum computation based on chiral Majorana fermions. *Proc. Natl Acad. Sci. USA* **115**, 10938-10942 (2018).
 - [36] Beenakker C.W.J. Theory of Coulomb-blockade oscillations in the conductance of a quantum dot. *Phys. Rev. B* **44**, 1646 (1991).
 - [37] Petta, J.R. *et al.* Coherent manipulation of coupled electron spins in semiconductor quantum dots. *Science* **309**, 2180-2184 (2005).
 - [38] Koppens, F.H.L. *et al.* Driven coherent oscillations of a single electron spin in a quantum dot. *Nature* **442**, 766-771 (2006).
 - [39] Zwanenburg, F.A. *et al.* Silicon quantum electronics. *Rev. Mod. Phys.* **85**, 961-1019 (2013).
 - [40] See Supplemental Material for details.
 - [41] Law, K. T., Lee, P. A. & Ng, T. K. Majorana fermion induced resonant Andreev reflection. *Phys. Rev. Lett.* **103**, 237001 (2009).
 - [42] Sun, Q.-F. & Xie, X.C. Quantum transport through a graphene nanoribbon/superconductor junction. *J. Phys.: Condens. Matter* **21**, 344204 (2009).
 - [43] Cheng, S.-G., Xing, Y.X., Wang, J. & Sun, Q.-F. Controllable Andreev Retroreflection and Specular Andreev Reflection in a Four-Terminal Graphene-Superconductor Hybrid System. *Phys. Rev. Lett.* **103**, 167003 (2009).
 - [44] Datta, S. *Electronic transport in mesoscopic system*. 102-110 (Cambridge University Press, 1995).

Acknowledgments

This work was financially supported by National Key R and D Program of China (2017YFA0303301), NBRP of China (2015CB921102), NSF-China (Grants No. 11574007), and the Key Research Program of the Chinese Academy of Sciences (Grant No. XDPB08-4).

Supplementary Materials

I. Scattering matrix for a system consisting of two chiral Majorana fermions coupled to a Majorana zero mode

Here we derive the scattering matrix of the chiral Majorana fermions (CMFs) in Fig.S1(a) (repeated from the main text for clarity) arising from the coupling with a Majorana zero mode (MZM). The properties of the CMFs are determined by the Hamiltonian H_1 defined in Eq.(2) of the main text. We begin by investigating the

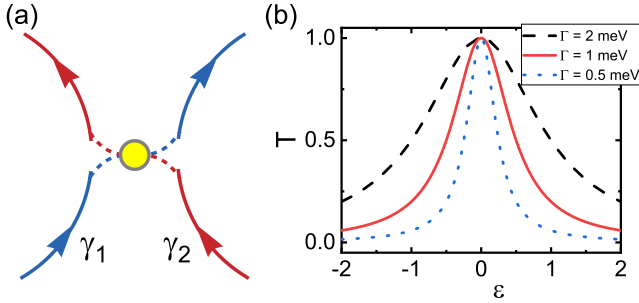


FIG. S1 . (a) Two CMFs γ_1 and γ_2 (blue and red arrows) are coupled to a MZM (yellow solid circle). (b) Transmission coefficient $T(\epsilon)$ for the scattering between γ_1 and γ_2 for different coupling strength $\Gamma_1 = \Gamma_2 = \Gamma$.

equations of motion for the field operators of the Ma-

jorana fermions, i.e., $i\partial_t \gamma_i(t) = [\gamma_i(t), H_1]$ ($i = 0, 1, 2$) in the Heisenberg picture. Then the operators obey the differential equations of motion

$$i\partial_t \gamma_\alpha(x, t) = 2i\nu \partial_x \gamma_\alpha(x, t) + it_\alpha \delta(x) \gamma_0(t), \quad (1)$$

$$i\partial_t \gamma_0(t) = - \sum_{\alpha=1,2} it_\alpha \gamma_\alpha(0, t). \quad (2)$$

Note that we have used the anticommutation relations $\{\gamma_\alpha(x), \gamma_\beta(x')\} = \delta_{\alpha\beta} \delta_{xx'}$ and $\{\gamma_0, \gamma_0\} = 1$ to derive these equations. By the Fourier transformation of $\gamma_\alpha(x, t)$ and $\partial_t \gamma_\alpha(x, t)$

$$\gamma_\alpha(x, \epsilon) = \int_{-\infty}^{+\infty} \gamma_\alpha(x, t) e^{i\epsilon t} dt, \quad (3)$$

$$\epsilon \gamma_\alpha(x, \epsilon) = \int_{-\infty}^{+\infty} [i\partial_t \gamma_\alpha(x, t)] e^{i\epsilon t} dt, \quad (4)$$

the differential equations (1) and (2) become

$$\epsilon \gamma_\alpha(x, \epsilon) = 2i\nu \partial_x \gamma_\alpha(x, \epsilon) + it_\alpha \delta(x) \gamma_0(\epsilon), \quad (5)$$

$$\epsilon \gamma_0(\epsilon) = - \sum_{\alpha=1,2} it_\alpha \gamma_\alpha(0, \epsilon). \quad (6)$$

Integrating the both side of Eq.(5) from 0^- to 0^+ , we obtain

$$2i\nu [\gamma_\alpha(0^+) - \gamma_\alpha(0^-)] + it_\alpha \gamma_0 = 0. \quad (7)$$

Here, the variable ϵ has been left out for simplicity. Using Eq.(6) and $\gamma_\alpha(0) = \frac{\gamma_\alpha(0^+) + \gamma_\alpha(0^-)}{2}$, one arrives at

$$(2i\nu + \frac{t_1^2}{2\epsilon})\gamma_1(0^+) + \frac{t_1 t_2}{2\epsilon} \gamma_2(0^+) = (2i\nu - \frac{t_1^2}{2\epsilon})\gamma_1(0^-) - \frac{t_1 t_2}{2\epsilon} \gamma_2(0^-), \quad (8)$$

$$\frac{t_1 t_2}{2\epsilon} \gamma_1(0^+) + (2i\nu + \frac{t_2^2}{2\epsilon})\gamma_2(0^+) = -\frac{t_1 t_2}{2\epsilon} \gamma_1(0^-) + (2i\nu - \frac{t_2^2}{2\epsilon})\gamma_2(0^-). \quad (9)$$

Denoting the incoming and outgoing scattering states of the CMFs by $\gamma_{1/2}(0^-)$ and $\gamma_{1/2}(0^+)$, respectively, the scattering matrix can be written as

$$\begin{pmatrix} \gamma_1(0^+) \\ \gamma_2(0^+) \end{pmatrix} = S_M \begin{pmatrix} \gamma_1(0^-) \\ \gamma_2(0^-) \end{pmatrix}. \quad (10)$$

Solving from Eqs.(8 and 9), we get the scattering matrix S_M as shown in Eq.(4) in the main text:

$$S_M = \frac{1}{A} \begin{pmatrix} 4i\epsilon\nu + t_1^2 - t_1^2 & -2t_1 t_2 \\ -2t_1 t_2 & 4i\epsilon\nu + t_1^2 - t_2^2 \end{pmatrix}, \quad (11)$$

in which $A = 4i\epsilon\nu + t_1^2 + t_2^2$ and ϵ is the incident energy. The off-diagonal elements of S_M matrix correspond to the amplitude for transmission between γ_1 and γ_2 . The resulting transmission coefficient is $T(\epsilon) = |S_{M,12}|^2 =$

$\frac{4\Gamma_1\Gamma_2}{4\epsilon^2 + (\Gamma_1 + \Gamma_2)^2}$ with $\Gamma_\alpha \equiv t_\alpha^2/(2\nu)$ which is same with the Breit-Wigner formula describing the resonant scattering of the lead/QD/lead system. For large ϵ , the transmission between γ_1 and γ_2 is forbidden ($T = 0$), while as ϵ approaching zero, a resonant exchange occurs which transform $\gamma_1 \rightarrow -\gamma_2$ and $\gamma_2 \rightarrow -\gamma_1$ ($T = 1$) as shown in Fig.S1(b).

II. Scattering matrix for a system consisting of two chiral Majorana fermions coupled to a quantum dot

Bellow, we derive the scattering matrix of the CMFs in Fig.S2 (repeated from the main text for clarity) arising from the coupling with a quantum dot (QD). In this

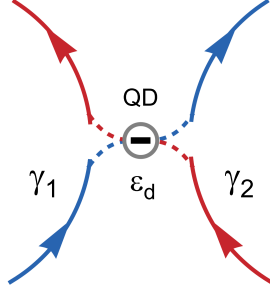


FIG. S2 . Two CMFs γ_1 and γ_2 (blue and red arrows) are coupled to a QD.

situation, the equation of motion for the field operators is $i\partial_t O(t) = [O(t), H_2]$, where $O(t)$ stands for the field operators of CMFs and the fermion state inside the QD in Heisenberg picture, and H_2 is defined in Eq.(5) of the main text. Here, the differential equations for the operators become

$$i\partial_t \gamma_\alpha(x, t) = 2i\nu \partial_x \gamma_\alpha(x, t) + i \frac{\tilde{t}_\alpha}{\sqrt{2}} \delta(x) [d(t) + d^\dagger(t)],$$

$$i\partial_t d(t) = \varepsilon_d d - \sum_{\alpha=1,2} i \frac{\tilde{t}_\alpha}{2} \gamma_\alpha(0, t),$$

$$i\partial_t d^\dagger(t) = -\varepsilon_d d^\dagger - \sum_{\alpha=1,2} i \frac{\tilde{t}_\alpha}{\sqrt{2}} \gamma_\alpha(0, t).$$

After a Fourier transformation similar to Eq.(3) and (4), we arrive at

$$\varepsilon \gamma_\alpha(x, \varepsilon) = 2i\nu \partial_x \gamma_\alpha(x, \varepsilon) + i \frac{\tilde{t}_\alpha}{\sqrt{2}} \delta(x) \gamma_0(\varepsilon), \quad (12)$$

$$\varepsilon d(\varepsilon) = \varepsilon_d d(\varepsilon) - \sum_{\alpha=1,2} i \frac{\tilde{t}_\alpha}{\sqrt{2}} \gamma_\alpha(0, \varepsilon), \quad (13)$$

$$\varepsilon d^\dagger(\varepsilon) = \varepsilon_d d^\dagger(\varepsilon) - \sum_{\alpha=1,2} i \frac{\tilde{t}_\alpha}{\sqrt{2}} \gamma_\alpha(0, \varepsilon). \quad (14)$$

Integrating the both side of Eq.(12) from 0^- to 0^+ , we obtain

$$2i\nu [\gamma_\alpha(0^+) - \gamma_\alpha(0^-)] + i \frac{\tilde{t}_\alpha}{\sqrt{2}} (d + d^\dagger) = 0. \quad (15)$$

Following the same procedure in the derivation of Eqs. (8,9,10), the scattering matrix S_Q for the QD coupling case can be found

$$S_Q = \frac{1}{\tilde{A}} \begin{pmatrix} \tilde{B} + \tilde{t}_2^2 - \tilde{t}_1^2 & -2\tilde{t}_1\tilde{t}_2 \\ -2\tilde{t}_1\tilde{t}_2 & \tilde{B} + \tilde{t}_1^2 - \tilde{t}_2^2 \end{pmatrix}, \quad (16)$$

where $\tilde{B} = 4i\nu(\varepsilon^2 - \varepsilon_d^2)/\varepsilon$ and $\tilde{A} = \tilde{B} + \tilde{t}_1^2 + \tilde{t}_2^2$. By setting $\varepsilon_d = 0$, the scattering matrix S_Q recovers S_M in Eq. (11). For finite ε_d , the transmission coefficient now becomes $\tilde{T}(\varepsilon) = |S_{Q,12}|^2 = \frac{4\tilde{\Gamma}_1\tilde{\Gamma}_2}{4(\varepsilon^2 - \varepsilon_d^2)^2 + (\tilde{\Gamma}_1 + \tilde{\Gamma}_2)^2}$ with $\tilde{\Gamma}_\alpha \equiv \tilde{t}_\alpha^2/(2\nu)$.

III. Calculation the transmission coefficients and terminal conductance in proposed devices

In this supplementary section, we give a detailed calculation of the transmission coefficients and terminal conductances of the proposed experimental devices for the observation of the braiding and its non-Abelian statistics.

A. Device that allows the observation of the braiding of chiral Majorana fermions

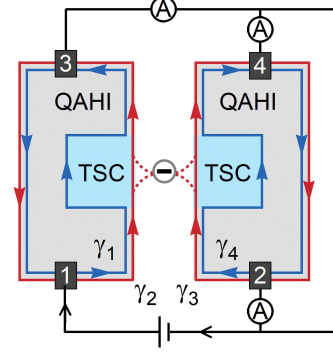


FIG. S3 . Experimental device that allows the observation of the braiding of chiral Majorana fermions based on TSC/QAHI junctions. Transport process via four chiral Majorana fermions γ_i . The chirality of γ_i in left junction is different with the one in right junction resulting from the opposite magnetization in two regions. The QD coupled to the TSC/QAHI junctions can trigger the exchange of γ_2 and γ_3 . The coupling strength is $\tilde{\Gamma}_1 = \tilde{\Gamma}_2 = \Gamma$.

First, we consider the device that allows the observation of the braiding of CMFs based on TSC/QAHI junctions in Fig.S3 (repeated from the main text for clarity). In the transport process of the four CMFs γ_i ($i = 1, 2, 3, 4$) in Fig.S3, γ_1 and γ_4 are transported directly into lead 3 and lead 4 while γ_2 and γ_3 are scattered by the QD. For simplicity, denoting the incoming CMFs by γ_2 and γ_3 , and outgoing scattering states by γ'_2 and γ'_3 respectively, the scattering matrix S_Q can be written as

$$\begin{pmatrix} \gamma'_2 \\ \gamma'_3 \end{pmatrix} = S_Q \begin{pmatrix} \gamma_2 \\ \gamma_3 \end{pmatrix}, \quad (17)$$

where S_Q is given by Eq. (16). We define four operators as

$$a_1 = (\gamma_1 + i\gamma_2)/\sqrt{2}, \quad (18)$$

$$a_2 = (\gamma_3 + i\gamma_4)/\sqrt{2}, \quad (19)$$

$$b_3 = (\gamma_1 + i\gamma'_2)/\sqrt{2}, \quad (20)$$

$$b_4 = (\gamma'_3 + i\gamma_4)/\sqrt{2}, \quad (21)$$

which represent the incoming QAHI edge modes (a_1 from lead 1 and a_2 from lead 2) and outgoing QAHI edge

modes (b_3 toward to lead 3 and b_4 toward to lead 4), respectively. By using Eq. (17), we can obtain

$$b_3 = [(1 + S_{Q,11})a_1 + (1 - S_{Q,11})a_1^\dagger + iS_{Q,12}a_2 + iS_{Q,12}a_2^\dagger]/2, \quad (22)$$

$$b_3^\dagger = [(1 - S_{Q,11}^*)a_1 + (1 + S_{Q,11}^*)a_1^\dagger - iS_{Q,12}^*a_2 - iS_{Q,12}^*a_2^\dagger]/2, \quad (23)$$

$$b_4 = [-iS_{Q,21}a_1 + iS_{Q,21}a_1^\dagger + (1 + S_{Q,22})a_2 + (-1 + S_{Q,22})a_2^\dagger]/2, \quad (24)$$

$$b_4^\dagger = [-iS_{Q,21}^*a_1 + iS_{Q,21}^*a_1^\dagger + (-1 + S_{Q,22}^*)a_2 + (1 + S_{Q,22}^*)a_2^\dagger]/2. \quad (25)$$

These equations can be rewritten into a compact form as

$$\begin{pmatrix} b_3 \\ b_3^\dagger \\ b_4 \\ b_4^\dagger \end{pmatrix} = \vec{S} \begin{pmatrix} a_1 \\ a_1^\dagger \\ a_2 \\ a_2^\dagger \end{pmatrix}, \quad (26)$$

with

$$\vec{S} = \frac{1}{2} \begin{pmatrix} 1 + S_{Q,11} & 1 - S_{Q,11} & iS_{Q,12} & iS_{Q,12} \\ 1 - S_{Q,11}^* & 1 + S_{Q,11}^* & -iS_{Q,12}^* & -iS_{Q,12}^* \\ -iS_{Q,21} & iS_{Q,21} & 1 + S_{Q,22} & -1 + S_{Q,22} \\ -iS_{Q,21}^* & iS_{Q,21}^* & -1 + S_{Q,22}^* & 1 + S_{Q,22}^* \end{pmatrix}. \quad (27)$$

Then the transport coefficients for normal tunneling and Andreev reflection from lead 1 to lead 3 and lead 4 can be obtained by

$$T_{31}(\varepsilon) = |\vec{S}_{11}|^2 = |1 + S_{Q,11}|^2/4, \quad (28)$$

$$T_{31}^A(\varepsilon) = |\vec{S}_{21}|^2 = |1 - S_{Q,11}^*|^2/4, \quad (29)$$

$$T_{41}(\varepsilon) = |\vec{S}_{31}|^2 = |iS_{Q,21}|^2/4, \quad (30)$$

$$T_{41}^A(\varepsilon) = |\vec{S}_{41}|^2 = |iS_{Q,21}^*|^2/4. \quad (31)$$

Considering the finite temperature \mathcal{T} , the effective transmission coefficients can be derived

$$T_{31} = \int_{-\infty}^{+\infty} T_{31}(\varepsilon) \left(-\frac{\partial f}{\partial \varepsilon}\right) d\varepsilon, \quad (32)$$

$$T_{31}^A = \int_{-\infty}^{+\infty} T_{31}^A(\varepsilon) \left(-\frac{\partial f}{\partial \varepsilon}\right) d\varepsilon, \quad (33)$$

$$T_{41} = \int_{-\infty}^{+\infty} T_{41}(\varepsilon) \left(-\frac{\partial f}{\partial \varepsilon}\right) d\varepsilon, \quad (34)$$

$$T_{41}^A = \int_{-\infty}^{+\infty} T_{41}^A(\varepsilon) \left(-\frac{\partial f}{\partial \varepsilon}\right) d\varepsilon, \quad (35)$$

in which $f(\varepsilon) = [\exp(\varepsilon/k_B\mathcal{T}) + 1]^{-1}$ is the Fermi distribution function.

Next, we assume that the voltage of lead 1 is set to be V and the voltage of lead 2,3,4 are the same assumed to be U . The measured current in lead n can be calculated using the multiprobe Landauer-Büttiker formula[42–44]

$$I_n = \frac{e^2}{h} \sum_m T_{nm}(V_n - V_m) + T_{nm}^A(V_n + V_m), \quad (36)$$

where T_{nm} (T_{nm}^A) is the normal tunneling (Andreev reflection) coefficient from lead m to lead n . The nonvanishing coefficients are $T_{13} = T_{24} = 1$ and T_{nm} (T_{nm}^A) with $n = 3, 4$ and $m = 1, 2$ which can be calculated from the scattering matrix \vec{S} as in Eqs.(32-35). With these coefficients, the currents of the leads are

$$I_1 = \frac{e^2}{h} T_{13}(V - U), \quad (37)$$

$$I_2 = 0, \quad (38)$$

$$I_3 = \frac{e^2}{h} [T_{31}(U - V) + T_{31}^A(U + V) + 2T_{32}^A U], \quad (39)$$

$$I_4 = \frac{e^2}{h} [T_{41}(U - V) + T_{41}^A(U + V) + 2T_{42}^A U]. \quad (40)$$

Then by the current conservation $I_1 + I_2 + I_3 + I_4 = 0$, one gets

$$U = \frac{T_{31} - T_{31}^A + T_{41} - T_{41}^A - T_{13}}{T_{31} + T_{31}^A + 2T_{32}^A + T_{41} + T_{41}^A + 2T_{42}^A - T_{13}} V. \quad (41)$$

The conductance of lead n is defined as $G_n = \frac{-I_n}{V_1 - V_n} = \frac{-I_n}{V - U}$, which can be obtained from Eqs.(37-41) straightforwardly.

B. Device for the observation of non-Abelian statistics

We now calculate the transport properties of the four CMFs after sequential exchanges. If the final state depends on the braiding order as well as the measurement of terminal conductance, this means that the braiding of CMFs obeys the non-Abelian statistics. First, we consider the joint operations with two exchanges, $\sigma_2\sigma_1$ and $\sigma_1\sigma_2$. $\sigma_2\sigma_1$ will transform the four CMFs according to $(\gamma_1, \gamma_2, \gamma_3, \gamma_4) \rightarrow (-\gamma_2, -\gamma_3, \gamma_1, \gamma_4)$. After the braiding, the outgoing QAHI edge modes (b_3 toward to lead 3 and b_4 toward to lead 4) now become

$$b_3 = (-\gamma_2 - i\gamma_3)/\sqrt{2} = (ia_1 - ia_1^\dagger - ia_2 - ia_2^\dagger)/2,$$

$$b_3^\dagger = (-\gamma_2 + i\gamma_3)/\sqrt{2} = (ia_1 - ia_1^\dagger + ia_2 + ia_2^\dagger)/2,$$

$$b_4 = (\gamma_1 + i\gamma_4)/\sqrt{2} = (a_1 + a_1^\dagger + a_2 - a_2^\dagger)/2,$$

$$b_4^\dagger = (\gamma_1 - i\gamma_4)/\sqrt{2} = (a_1 + a_1^\dagger - a_2 + a_2^\dagger)/2,$$

in which we have used $\gamma_1 = \frac{1}{\sqrt{2}}(a_1 + a_1^\dagger)$, $\gamma_2 = \frac{1}{i\sqrt{2}}(a_1 - a_1^\dagger)$, $\gamma_3 = \frac{1}{\sqrt{2}}(a_2 + a_2^\dagger)$, $\gamma_4 = \frac{1}{i\sqrt{2}}(a_2 - a_2^\dagger)$. Now, the scattering matrix \vec{S} relating the incoming modes $a_{1,2}, a_{1,2}^\dagger$ and $b_{3,4}, b_{3,4}^\dagger$ becomes

$$\vec{S} = \frac{1}{2} \begin{pmatrix} i & -i & -i & -i \\ i & -i & i & i \\ 1 & 1 & 1 & -1 \\ 1 & 1 & -1 & 1 \end{pmatrix},$$

which gives $T_{31} = T_{41} = T_{31}^A = T_{41}^A = 1/4$ and $T_{32} = T_{42} = T_{32}^A = T_{42}^A = 1/4$. By using these normal tunneling and Andreev reflection coefficients, the conductances can be obtained from Eqs.(37-41), and the results are that $G_3 = G_4 = \frac{e^2}{2h}$. Similarly, the scattering matrix for the joint operation $\sigma_1\sigma_2$ can be obtained following the same procedure as

$$\vec{S} = \frac{1}{2} \begin{pmatrix} i & i & 1 & 1 \\ -i & -i & 1 & 1 \\ -i & i & 1 & -1 \\ -i & i & -1 & 1 \end{pmatrix},$$

thus it gives the same terminal conductance $G_3 = G_4 = \frac{e^2}{2h}$ as $\sigma_2\sigma_1$ despite that the final states are different.

Next, we turn to the joint operators $\sigma_2\sigma_1\sigma_2$ and $\sigma_2\sigma_2\sigma_1$. After the transformation by $\sigma_2\sigma_1\sigma_2$, $(\gamma_1, \gamma_2, \gamma_3, \gamma_4)$ becomes $(\gamma_3, -\gamma_2, \gamma_1, \gamma_4)$, and the resulting scattering matrix is

$$\vec{S} = \frac{1}{2} \begin{pmatrix} -1 & 1 & 1 & 1 \\ 1 & -1 & 1 & 1 \\ 1 & 1 & 1 & -1 \\ 1 & 1 & -1 & 1 \end{pmatrix}.$$

We obtain $T_{31} = T_{41} = T_{31}^A = T_{41}^A = 1/4$ and $T_{32} = T_{42} = T_{32}^A = T_{42}^A = 1/4$, and $G_3 = G_4 = \frac{e^2}{2h}$ again. However, the joint operator $\sigma_2\sigma_2\sigma_1$ transforms the CMFs γ_i according to $(\gamma_1, \gamma_2, \gamma_3, \gamma_4) \rightarrow (-\gamma_2, -\gamma_1, -\gamma_3, \gamma_4)$. The related scattering matrix now becomes

$$\vec{S} = \frac{1}{2} \begin{pmatrix} 0 & -i & 0 & 0 \\ i & 0 & 0 & 0 \\ 0 & 0 & 0 & -1 \\ 0 & 0 & 1 & 0 \end{pmatrix},$$

which gives $T_{31}^A = T_{42}^A = 1$ and $T_{31} = T_{41} = T_{41}^A = T_{32} = T_{42} = T_{42}^A = 0$. The corresponding terminal conductances are $G_4 = \frac{e^2}{h}$ and $G_3 = 0$. At this point, we can see that not only the two joint operators $\sigma_2\sigma_1\sigma_2$ and $\sigma_2\sigma_2\sigma_1$ drive the CMFs γ_i from the same initial state into different final states, but also the resulting terminal conductance is distinct. These results provide a method to observe the non-Abelian braiding statistics of the CMFs.

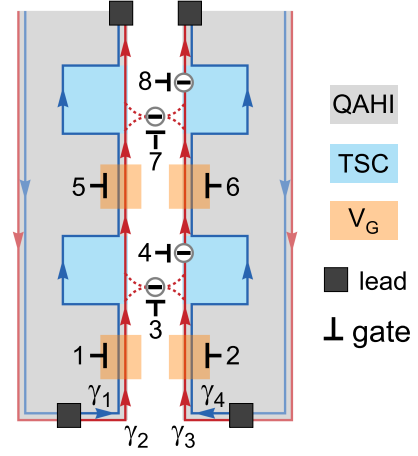


FIG. S4. An universal device that allows various braiding operations by tuning the gates based on TSC/QAHI junctions. The pair of QDs between the two TSC regions are used to carry out σ_2 as discussed in the main text. The gate voltages V_G placed on the QAHI edge are used to carry out σ_1 and σ_3 . The QDs and gated regions are controlled by gates.

IV. An universal device for executing various braiding operations in an electrically controllable manner

As discussed in the main text, the coupling with QDs provides an electrical control of the braiding of CMFs. In this final section, we further propose an universal device for executing various braiding operations controlled by gates as shown in Fig.S4 to show the advantages of our strategy. Similar to the devices in Fig.4 of the main text, the device as shown in Fig.S4 is made by two ribbons of hybrid TSC/QAHI junctions with opposite out-plane magnetization. Here, we introduce four QAHI regions covered by gate voltage V_G as denoted by orange shadow regions to carry out the braiding operator σ_1 (σ_3) controlled by gate 1 and 5 (2 and 6)[35]. Moreover, four QDs controlled by gate 3,4,7,8 are placed between the TSC regions to carry out the braiding operator σ_2 . If all the operators controlled by the gates are working, the operation realized in Fig.S4 is $\sigma_2\sigma_3\sigma_1\sigma_2\sigma_3\sigma_1$ and transforms the four CMFs $(\gamma_1, \gamma_2, \gamma_3, \gamma_4)$ into $(-\gamma_4, \gamma_3, -\gamma_2, \gamma_1)$. The advantage of our proposed device is that all the modules to realize the braiding operators are electrically controllable and this point makes various operations available in a single device by tuning the gates.

In principle, there are 64 (2^6) combinations of σ_i ($i = 1, 2, 3$) which can be executed by the device in Fig.S4. Here, we show four representative operations in Fig.S5. If one tunes the gates 1,2,6 away from the working conditions for the braiding operators σ_1 and σ_3 , then the resulting operation is $\sigma_2\sigma_1\sigma_2$ as shown in Fig.S5(a), i.e., the joint operation in Fig.4a of the main text. Similarly, the joint operation $\sigma_2\sigma_2\sigma_1$ in Fig.4b of the main text can be

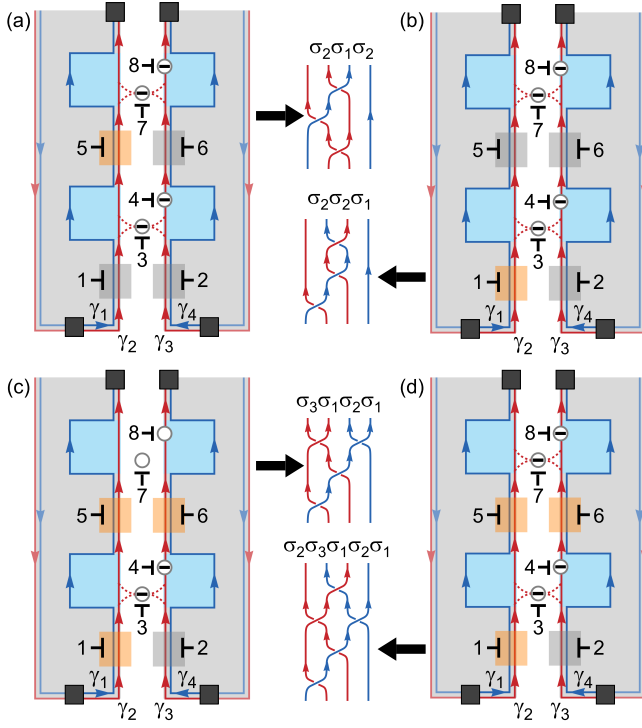


FIG. S5 . Four representative operations realized in the device from Fig.S4 by tuning the gates. (a) By tuning the gates 1,2,6 away from the working conditions as represented by dark gray shadow regions, the resulting operation recovers $\sigma_2 \sigma_1 \sigma_2$ in Fig.4(a) of the main text. (b) the operation $\sigma_2 \sigma_2 \sigma_1$ by tuning gates 2,5,6, reminiscent of Fig.4(b) in the main text. (c) and (d) the operations $\sigma_3 \sigma_1 \sigma_2 \sigma_1$ and $\sigma_2 \sigma_3 \sigma_1 \sigma_2 \sigma_1$. The hollow circles in (c) means that the energy level ε_d is tuned away from zero by gate 7,8 and the QDs cannot braid the CMFs anymore. The middle part shows the corresponding braiding of γ_i ($i = 1, 2, 3, 4$).

carried out by tuning the gates 2,5,6 away from the working conditions as shown in Fig.S5(b). Moreover, as shown in the main text, if the energy level ε_d of the QDs deviates from zero, the braiding of CMFs is unrealizable as indicated by hollow circle in Fig.S5(c). In Fig.S5(c), we disable the QDs controlled by gate 7,8 and the V_G controlled by gate 2, then the consequent operation $\sigma_3 \sigma_1 \sigma_2 \sigma_1$ transform $(\gamma_1, \gamma_2, \gamma_3, \gamma_4)$ into $(\gamma_3, -\gamma_2, -\gamma_4, \gamma_1)$. If we switch on the QD again as shown in Fig.S5(d), another operation $\sigma_2 \sigma_3 \sigma_1 \sigma_2 \sigma_1$ is achieved and the CMFs $(\gamma_1, \gamma_2, \gamma_3, \gamma_4)$ are transformed to $(\gamma_3, \gamma_4, -\gamma_2, \gamma_1)$. The remaining operations can be also achieved by tuning the corresponding gates.